This article is published in ACS Applied Nanomaterials (ACS Appl. Nano Mater., 2022, DOI: 10.1021/acsanm.2c00035), which should be cited to refer to this work.

Salt-Templated Solvothermal Synthesis of Dioxane-Linked Three-Dimensional Nanoporous Organic Polymers for Carbon Dioxide and Iodine Capture

Timur Ashirov, Kyung Seob Song, and Ali Coskun*

ABSTRACT: Precise control over the textural properties of porous organic polymers, POPs, is a daunting task, yet highly important to achieve the desired porosity and pore connectivity for target applications. Accordingly, the introduction of hard templates in the solvothermal synthesis of POPs could help to control the surface area and pore size without altering their chemical structure. In this direction, here we synthesized a dioxane-linked three-dimensional tetraphenylene-based nanoporous organic polymer (3D-tPOP) using low-cost and readily available NaCl salt as a hard template under solvothermal conditions. The presence of a hard template enhanced the surface area and enabled control over the morphology, micropore/mesopore ratio, and pore volume with respect to the template amount. Whereas micron-sized NaCl templates facilitated the surface growth of a microporous polymer network, nanosized NaCl crystallites led to the formation of mesopores. The resulting 3D-tPOPs showed tunable micropore/mesopore ratios and surface areas in the range of 349−1058 $m^2\ g^{-1}$ with a linear correlation to the template amount. A high CO_2 uptake capacity of 5.02 mmol g^{-1} at 273 K and 1 bar and an I_2 uptake capacity of 1180 mg g^{-1} were observed for 3D-tPOPs with micropore and mesopore ratios of 50.2% and 71.4%, respectively.

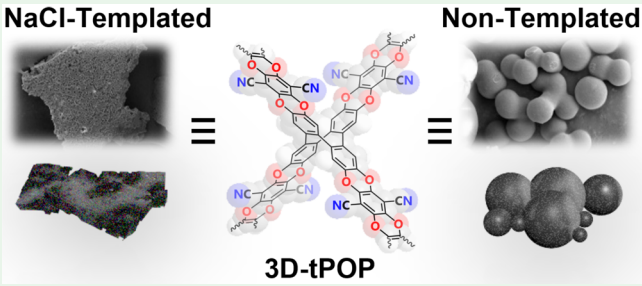

KEYWORDS: *porous organic polymers, porosity control, CO_2 capture, I_2 uptake, solvothermal synthesis*

1. INTRODUCTION

Increasing industrialization and associated carbon dioxide (CO_2) emissions have already had observable effects on the environment.[1] Therefore, the development of efficient sorbents for CO_2 capture is not only vital for environmental protection but also important for the development of a CO_2 circular economy, which involves the further utilization of captured CO_2 as a sustainable chemical commodity.[2] In this direction, porous organic polymers (POPs) have been considered as promising alternatives for CO_2 capture and separation because of their structural tunability, high porosity, and chemical stability.[3−7] Moreover, POPs have also found applications in atmospheric water capture,[8] semiconducting materials,[9] heterogeneous catalysis,[10] precious metal recovery, water purification, iodine (I_2) capture, and many others.[11,12] The structural tunability of POPs allows one to control the nature of chemical functionalities by choosing suitable precursors.[13−15] The porosity and pore size of POPs, on the other hand, are determined by the length, dimensions, and rigidity of the building block as well as the degree of interpenetration of the polymer backbone.[16] Hence, the ability to control the porosity, especially in three-dimensional (3D) POPs, is essential for the design of new polymers with the desired porosity for target applications. One promising strategy to control the pore size and surface area in POPs is the use of hard and/or soft templates, which can be removed once the network is formed.[17] In this direction, the nature of the template has a profound impact in the porosity of POPs. For example, one of the commonly used templates is alkali-metal salts. Eutectic salt mixtures of alkali-metal salts and zinc dichloride[18,19] have been used as soft templates to control the porosity of covalent triazine frameworks[20] and covalent isocyanurate frameworks under ionothermal conditions.[19] Notably, for the latter example, the presence of alkali-metal salts enabled a strong template effect for the formation of a microporous network even at high reaction temperatures of 500 °C. Nonetheless, these polymerization reactions require high temperatures, which result in partial carbonization of the polymer network.[14,15,17] The solvothermal synthesis, on the other hand, proceeds at much lower temperatures and provides better structural control. The templated synthesis of POPs under solvothermal conditions, however, is not well under-

stood. To date, very few examples of the salt-templated synthesis under solvothermal conditions have been reported.[21,22] Li and co-workers used silica hard templates of SBA-15 and B56-E-20 as templates to grow hierarchically porous frameworks under solvothermal conditions.[23] In this approach, however, the preparation of frameworks with different porosities requires different templates.[23] In a recent example, Shi and co-workers[24] used table salt (NaCl) as a template for the synthesis of covalent organic nanosheets with different thicknesses and lateral sizes, which were grown on the template surface. Various alkali-metal salts have also been used as modulators to tune the Hansen solubility parameters of the solvents in the solvothermal synthesis to control the porosity in microporous organic polymers.[21,22] Precise control over the textural properties of POPs using the same monomers is of great importance in tuning of the porosity of these polymers for the desired applications. In this direction, we reasoned that favorable interactions between the monomer and hard template such as NaCl could promote surface growth, thus enabling control over the porosity of the resulting POPs. We identified trimethylsilane (TMS)-protected octahydroxytetraphenylene (OTMSTP) as the ideal building block to promote 3D network growth because of its negative curvature, conjugated nature, and high free volume.[25,26] The polymerization of OTMSTP with 2,3,5,6-tetrafluoroterephthalonitrile (TFPN)[27] through nucleophilic aromatic substitution (SNAr) reaction was performed in the presence of a catalytic amount of tetrabutylammonium fluoride (TBAF) and varying amounts of NaCl as a hard template, enabling control over the pore size and porosity of the resulting polymers, named 3D-tPOPs, starting from the same monomer. Notably, by gradually changing the NaCl amount, we were able to tune the ratio of the micro- and mesopores as well as the CO_2 and I_2 uptake capacities of 3D-tPOPs (Scheme 1). 3D-tPOPs prepared by

Scheme 1. Synthetic Pathway for the Preparation of 3D-tPOPs through the Polymerization of OTMSTP and TFPN Using TBAF as a Catalyst under Solvothermal Conditions with and without a NaCl Template[a]

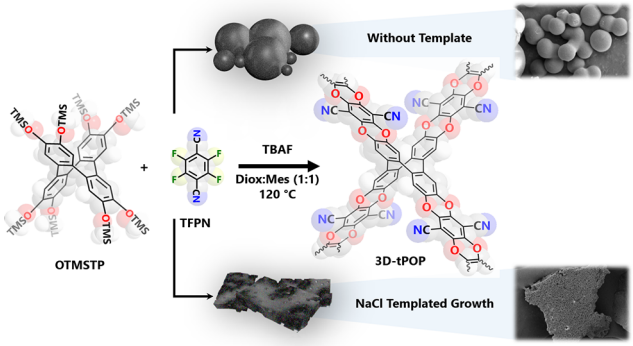

[a]The template has a profound impact on the polymer morphology and growth, as shown in the SEM images.

the templated synthesis under solvothermal conditions showed tunable surface areas at 349 and 1058 $m^2\ g^{-1}$ along with the highest CO_2 uptake capacity of 5.02 mmol g^{-1} at a micropore ratio of 50.2% and a high I_2 uptake capacity of 1180 mg g^{-1} at a mesopore ratio of 71.4%.

2. RESULTS AND DISCUSSION

The synthesis of octahydroxytetraphenylene was performed by following the previously reported literature procedure.[25,28,29] This precursor was subsequently protected with trimethylsilane (TMS) to form OTMSTP to increase the solubility of the monomer. Moreover, the cyclooctatetraene core of OTMSTP is inherently nonplanar because of its antiaromaticity, thus providing an ideal geometry to form a 3D network. The polymerization reaction between OTMSTP and TFPN was carried out under solvothermal conditions using a 1:1 mixture of 1,4-dioxane and mesitylene (1.0 mL) and TBAF as a catalyst at 120 °C for 3 days. NaCl was used in the amounts ranging from 0.25 to 2.0 g as a hard template to control the porosity (sample name: 3D-tPOP-NaCl-X, where X corresponds to the amount of NaCl added in grams). Importantly, *in situ* deprotection of the TMS group of OTMSTP using TBAF promoted the formation of 3D-tPOP through SNAr reaction, while also increasing the affinity of the monomer toward the template surface through ion−ion and ion−dipole interactions, thus facilitating the surface growth of the polymer network.

The formation of 3D-tPOPs was confirmed by using Fourier transform infrared (FTIR) spectroscopy analysis (Figure 1a). The FTIR spectra revealed the disappearance of C−F vibration bands of TFPN and $-Si(CH_3)_3$ signals of OTMSTP at ∼1317 and ∼832 cm^{-1}, respectively.[30,31] Moreover, the appearance of the C−O stretching band at ∼1254 cm^{-1} along with the retention of nitrile stretching band at ∼2253 cm^{-1} verified the formation of 3D-tPOPs.[30,32] In addition, the disappearance of the −C−O−Si− vibration band at ∼1172 cm^{-1} further confirmed the successful polymerization.[33] Interestingly, the intensities of the −C−H and −Si−C− stretching bands at ∼2956 and ∼740 cm^{-1}, respectively, for the polymers prepared through the templated synthesis are lower compared to those for the nontemplated sample (Figure S6), implying a higher degree of polymerization in the templated samples.[33] We also characterized (Figure 1b) the molecular connectivity of 3D-tPOPs using X-ray photoelectron spectroscopy (XPS) analysis. The XPS survey spectra of 3D-tPOPs revealed only carbon, nitrogen, oxygen, and silicon along with negligible amounts of fluorine and chlorine (Figure S8). The XPS C 1s spectrum of 3D-tPOP-NaCl-1.0 revealed the peaks for sp^2 carbon at 284.8 eV, the −C−O−C− (dioxane linkages) at 286.4 eV, and the −C≡N at 287.0 eV.[30,32] Additionally, the −C−Si− peak at 284.2 eV and the −C−O− peak at 285.8 eV, which correspond to the residual end groups of the polymers, can also be observed.[34] On the other hand, the XPS N 1s spectrum of 3D-tPOP-NaCl-1.0 revealed only a single peak at 399.8 eV corresponding to −C≡N, further confirming the preservation of nitrile groups.[30] Moreover, the XPS O 1s spectrum showed the presence of three types of oxygen moieties at 531.4, 533.4, and 534.5 eV matching with the −O−Si−, −C−O−C−, and −C−O− binding energies.[32,35] The XPS Si 2p spectrum showed only two types of peaks at 101.5 and 102.7 eV fitting to the −Si−C− and −Si−O−C− bonds, respectively.[34] In order to verify the chemical structure of 3D-tPOPs, we also measured the ^1H and ^{13}C cross-polarization magic-angle-spinning (CP-MAS) NMR spectra of 3D-tPOPs (Figure S7). The ^1H MAS NMR spectra of 3D-tPOPs revealed the presence of two peaks at ∼2.3 and 8.2 ppm corresponding to the TMS and aromatic protons, respectively. The higher intensity of the TMS protons in the case of 3D-tPOP indicates incomplete polymerization, which is in good agreement with the FTIR

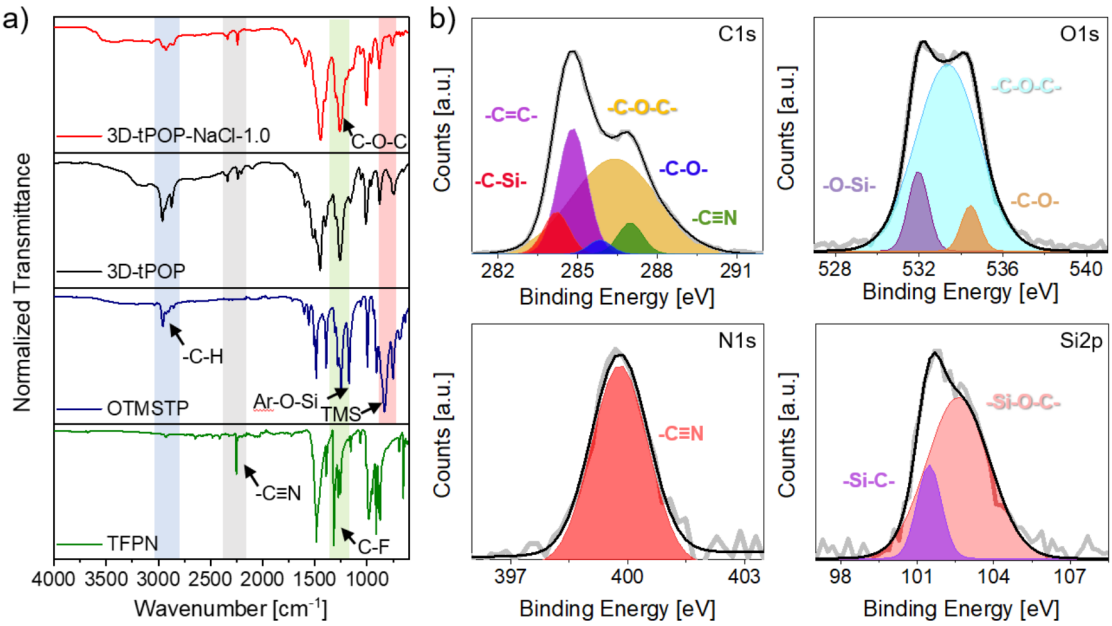

Figure 1. (a) FTIR spectra of 3D-tPOP, 3D-tPOP-NaCl-1.0 and corresponding monomers, OTMSTP, and TFPN. (b) XPS C 1s, O 1s, N 1s, and Si 2p spectra of 3D-tPOP-NaCl-1.0.

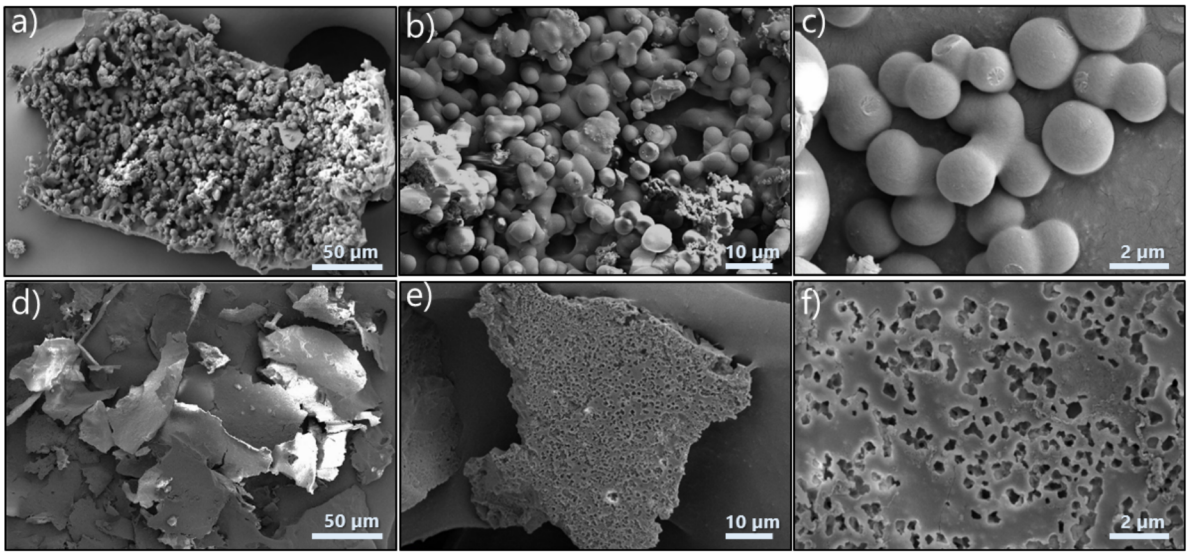

Figure 2. SEM images of 3D-tPOP prepared without template (a−c) and 3D-tPOP-NaCl-1.0 prepared using 1.0 g of the NaCl template (d−f). The SEM images clearly show significant differences between the growth structures with and without the NaCl template.

results (Figure S6). The intensity of the aromatic protons, on the other hand, were found to be higher for the NaCl-templated samples, further supporting the fact that templation leads to a higher degree of polymerization. Similarly, the ^{13}C CP-MAS NMR spectra of 3D-tPOPs revealed the presence of a large number of TMS moieties between ∼15 and 25 ppm. All of the polymers showed carbon signals at ∼96, ∼118, and ∼140 ppm assigned to the carbon atoms connected to the nitrile moieties, aromatic carbons, and −C−O− moieties, respectively (Figure S7b).[30] These results verify the formation of 3D-tPOPs. In order to probe the elemental composition of 3D-tPOPs, we performed elemental analysis (EA). The EA results revealed (Table S1) that the elemental composition of the 3D-tPOP-NaCl-X samples is very close to the calculated value, except for the 3D-tPOP prepared in the absence of template, which suggests incomplete polymerization as also observed in the FTIR and NMR analyses (Figures S6 and S7). The slightly higher hydrogen content was attributed to the OTMS end groups and water molecules trapped in the pores of the 3D-tPOPs.

The X-ray diffraction (XRD) patterns revealed that the 3D-tPOP prepared without a template is amorphous with a broad diffraction peak at ∼21.2°, which was attributed to $\pi-\pi$ stacking within the polymer network (Figure S9).[30] This peak, however, decreased significantly for polymers synthesized in the presence of NaCl, thus suggesting a decreased degree of interpenetration (Figure S10). Thermogravimetric analysis (TGA) was performed under a nitrogen atmosphere to probe the thermal stability of 3D-tPOPs. Interestingly, 3D-tPOPs synthesized in the absence of a template showed a

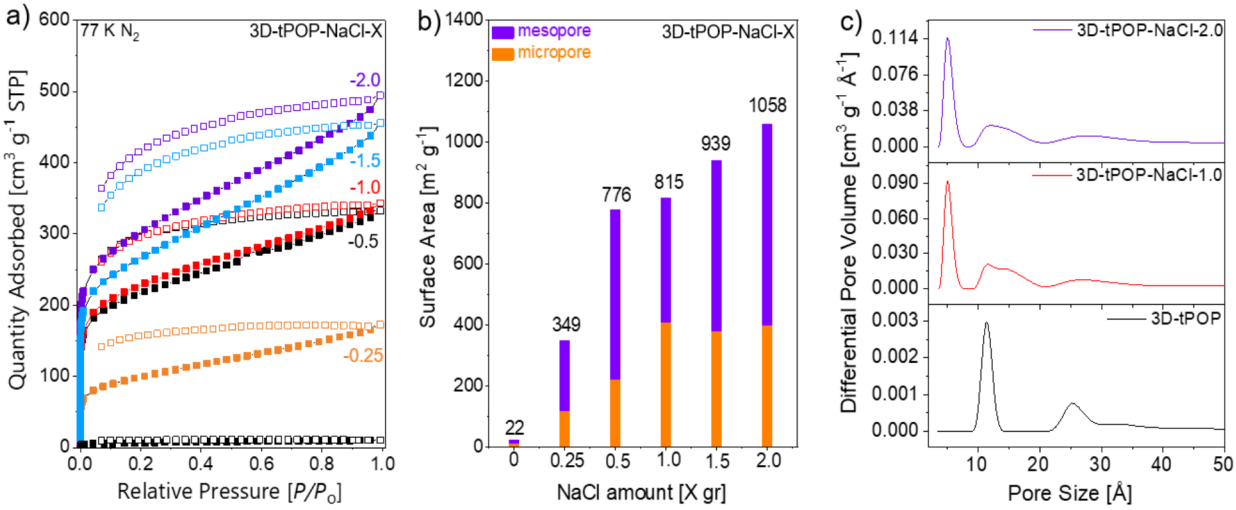

Figure 3. Porosity analysis of 3D-tPOPs: (a) N_2 adsorption−desorption isotherms of the 3D-tPOP and 3D-tPOP-NaCl samples measured at 77 K. The values near the isotherms represent the corresponding amount of the NaCl template used in grams. The filled and empty symbols correspond to adsorption and desorption, respectively. (b) Change of the BET surface area in terms of the ratio of the micro/mesopores versus NaCl amount. (c) NLDFT PSD versus differential pore volume curves for the 3D-tPOP and 3D-tPOP-NaCl-1.0 and -2.0 samples.

Table 1. Porosity, Pore Volume, and Meso- and Microporosity Analysis of the 3D-tPOP and 3D-tPOP-NaCl Samples Obtained from N_2 Adsorption−Desorption Isotherms at 77 K

sample name	S_{BET}[a] (m^2 g^{-1})	Langmuir (m^2 g^{-1})	S_{micro}[b] (m^2 g^{-1})	S_{ext} (m^2 g^{-1})	V_{total}[c] (cm^3 g^{-1})	V_{micro}[d] (cm^3 g^{-1})	ratio of S_{micro} (%)	ratio of S_{ext} (%)
3D-tPOP	22	29						
3D-tPOP-NaCl-0.25	349	436	119	230	0.27	0.05	34.1	65.9
3D-tPOP-NaCl-0.5	776	943	222	554	0.50	0.10	28.6	71.4
3D-tPOP-NaCl-1.0	815	995	409	406	0.54	0.18	50.2	49.8
3D-tPOP-NaCl-1.5	939	1160	380	559	0.66	0.17	40.5	59.5
3D-tPOP-NaCl-2.0	1058	1316	399	659	0.77	0.18	37.7	62.3

[a]The BET surface area was calculated over the linear pressure range (P/P_0) of 0.01−0.18. [b]The micropore area was calculated from the N_2 adsorption isotherms by applying the *t*-plot method. [c]The total pore volume was obtained at P/P_0 = 0.99. [d]The micropore volume was calculated by applying the *t*-plot method.

significant weight loss at ∼190 °C, which points to the existence of mostly oligomers and incomplete polymerization due to the low solubility of the OTMSTP monomer following *in situ* deprotection (Figure S11). However, the TGA plots of the 3D-tPOPs synthesized in the presence of NaCl showed much improved thermal stabilities up to ∼350 °C, thus suggesting the existence of surface-templated growth of the polymer network and possibly the improved solubility parameter of the reaction solvent. TGA performed under air also showed similar results (Figure S12) with a 100% weight loss at ∼550 °C, thus confirming complete removal of inorganic salts. Scanning electron microscopy (SEM) images were collected (Figures 2 and S13) to observe the impact of the template on the morphologies of the 3D-tPOPs. In the absence of a template, the SEM images of 3D-tPOP showed (Figure 2a−c) spherical particles with sizes ranging from 3 to 5 μm, which is commonly observed for POPs. On the other hand, the morphology of the samples prepared by the template approach turned out to be completely different; 3D-tPOP-NaCl-1.0 exhibited a highly porous sheet-like morphology, and the cubic-shaped pores originating from NaCl crystallites can also be seen (Figure 2d−f) in the SEM images, thus suggesting the surface growth of the polymer networks. Importantly, a similar sheetlike morphology is consistently observed (Figure S13) in the SEM images of all of the 3D-tPOPs prepared using different NaCl amounts. In order to better understand the effect of the NaCl template on the polymer morphology and to observe the distribution of the NaCl crystallites within the polymer structure, we performed (Figures S14 and S15) transmission electron microscopy (TEM) analysis of 3D-tPOPs without removing the salt. The TEM images revealed the coexistence of nanometer-sized NaCl crystallites along with the micron-sized ones in the 3D-tPOP-NaCl-1.0 sample (Figure S15).

The porosity of 3D-tPOPs was evaluated using N_2 adsorption−desorption measurements performed at 77 K (Figure 3a). The respective surface areas of the 3D-tPOPs were calculated according to the Brunauer−Emmett−Teller (BET) theory from the adsorption isotherms at pressure ranges determined from the Rouquerol plots (Figures S16 and S17).[36] 3D-tPOP showed a very low BET surface area of 22 m^2 g^{-1}, which can be attributed to a lower degree of polymerization, as indicated by the low decomposition temperature in TGA measurements. In contrast, the NaCl-templated samples (3D-tPOP-NaCl-X samples) showed good surface areas ranging from 349 to 1058 m^2 g^{-1} with characteristic type I adsorption isotherms, indicating the highly microporous structures of the polymers.[37] The combination of H4 and broad hysteresis loop in the desorption branch covering the entire pressure range points to the presence of mesopores and

to the swelling of the polymer network due to its flexibility, respectively.[38] The BET surface area of the 3D-tPOP-NaCl samples increased proportionally with the template amount (Table 1). Similarly, the micropore surface area also increased with the template amount and reached a plateau at 409 m^2 g^{-1} for 3D-tPOP-NaCl-1.0 (Figure 3b). The samples prepared using higher amounts of NaCl showed similar micropore surface areas accompanied by increasing mesopore content proportional to the template amount. Likewise, the pore volume also increased, with the template amount reaching to 0.77 cm^3 g^{-1} for the 3D-tPOP-NaCl-2.0 sample. The pore-size distribution (PSD) of the 3D-tPOPs was evaluated (Figure 3c) using the nonlocal density functional theory (NLDFT) model based on the carbon standard slit model. PSD analysis of the 3D-tPOP showed the existence of 11.4- and 25.2-Å-sized pores in the micropore and mesopore ranges, respectively. However, in the samples prepared by the NaCl-templated synthesis, a new 5.1 Å pore in the ultramicropore region emerged along with the 11.4-Å-sized pores (Figures 3c and S18).[39] Moreover, the pore volume also increased with the template amount (Table 1). The formation of abundant micropores is ascribed to the surface growth of the polymer networks on the NaCl crystallites. The mesoporosities of the 3D-tPOP samples were also analyzed using the Barrett−Joyner−Halenda (BJH)[40] method (Figure S19). BJH analysis revealed the presence of mesopores ranging from 3 to 15 nm, the amount of which increased proportionally to the template amount. Although the solubility of NaCl at room temperature in 1,4-dioxane is extremely low,[41] the temperature of the reaction and addition of tetrahydrofuran (THF) can possibly solubilize small amounts NaCl salt, leading to the formation of nanometer-sized NaCl crystallites (Figure S15).[42] Accordingly, we attribute the increase in the mesopore content with increasing template loading to the higher amount of nanosized NaCl crystallites, which promote the formation of mesopores.

In order to probe the impact of the template approach on the CO_2 affinity and uptake capacity, we measured the CO_2 adsorption isotherms of the 3D-tPOPs at different temperatures, 273, 298, and 323 K, and also calculated the isosteric heats of adsorption (Q_{st}) of CO_2 to compare the CO_2 affinities of the polymers (Table 2). Even though the 3D-tPOP showed a very low porosity, it still showed a CO_2 uptake capacity of 2.38 mmol g^{-1} at 273 K due to the presence of dioxane and nitrile moieties (Figure 4a). The polymers synthesized by the template approach showed higher CO_2 uptake capacities ranging from 3.24 to 5.02 mmol g^{-1}, with 3D-tPOP-NaCl-1.0 being the highest (Figure 4a). Interestingly, 3D-tPOP-NaCl-1.5 and -2.0 exhibited lower CO_2 uptake capacities compared to 3D-tPOP-NaCl-1.0. The CO_2 adsorption at 273 and 298 K nicely followed the micropore ratio [S_{micro} (%); Table 1].

3D-tPOP-NaCl-1.0 exhibited the highest micropore ratio of 50.2% and thus the highest CO_2 uptake capacity, 5.02 mmol g^{-1} (Figure 4b).[44−46] Remarkably, by a simple change in the amount of template, it is possible to control the CO_2 uptake capacity, thus presenting another dimension for controlling the porosity of POPs for the desired application. Finally, to evaluate the CO_2 affinity of 3D-tPOPs, we calculated the Q_{st} value of CO_2 for 3D-tPOPs (Figure 4c). The Q_{st} value of the 3D-tPOP was found to be 25.8 kJ mol^{-1} at zero coverage. The Q_{st} values of the 3D-tPOP-NaCl samples prepared by the templated synthesis approach, however, ranged from 39.3 to 43.2 kJ mol^{-1} (Table 2). These high isosteric heat of adsorption values originated from the dipole−quadrupole interactions between nitrile moieties and dioxane linkages with CO_2 molecules as well as the large abundance of ultramicropores.[47,48] The isosteric heat of adsorption values are ideal for CO_2 capture through physisorption and thus do not require high energy for CO_2 desorption.[43] The calculated heat of adsorption values are higher than most of the previously reported POPs (Table S2).[14,19,49] These results show that readily available, cheap salts such as NaCl can be used to tune the properties of the polymers by increasing both the porosities and gas uptake capacities.

In order to further elaborate on the versatility of the templated synthesis approach, we also explored the I_2 uptake capability of the 3D-tPOPs. Iodine has radioactive isotopes, namely, ^{129}I and ^{131}I, which are produced as waste in nuclear power plants.[50] Therefore, the capture and immobilization of radioiodines is very important because of their very long half-life and adverse effects on human health. In this regard, POPs have already emerged as suitable candidates for I_2 capture; however, a direct correlation between the I_2 uptake capacity and porosity would be helpful for the design of new sorbents.[51−53] In this direction, we performed vapor-phase I_2 uptake measurements for the 3D-tPOPs, simulating the nuclear waste reprocessing conditions (Figure S22).[54] Remarkably, the 3D-tPOPs showed exceptional I_2 uptake capacities up to 1180 mg g^{-1} along with fast uptake kinetics, which are comparable to those of the best-performing POPs (Figure 4d,e and Table S3).[53] Contrary to the CO_2 uptake experiments, 3D-tPOP-NaCl-0.5 showed the highest I_2 uptake capacity. The I_2 uptake capacity depends on several factors such as the chemical structure, porosity, and pore volume.[55] Because the chemical structures of the 3D-tPOPs are same, the variation in the uptake capacity can only be attributed to the differences in the porosities. Indeed, we found a clear correlation between the I_2 uptake capacity and the mesopore ratio [S_{ext} (%); Table 1] of the 3D-tPOPs (Figure 4d); the highest mesopore ratio of 71.4% was observed for 3D-tPOP-NaCl-0.5 along with the highest I_2 capture capacity. Because iodine has a relatively large kinetic diameter (∼5 Å), it initially diffuses into the mesopores.[51,52] Accordingly, 3D-tPOPs prepared by the templated synthesis showed very fast uptake kinetics, with more than 70% of I_2 uptake happening within 60 min governed by the presence of mesopores (Figure 4e). We can, however, see the difference in the I_2 uptake capacities and a clear correlation with the mesopore ratio after prolonged exposure to I_2. We reasoned that the higher mesopore ratio not only

Table 2. CO_2 Uptake Capacities at Different Temperatures and Isosteric Heats of Adsorption Results of the 3D-tPOPs and 3D-tPOP-NaCl Polymers

sample name	CO_2 uptake (mmol g^{-1}) T = 273 K	T = 298 K	T = 323 K	Q_{st}[a] (kJ mol^{-1})
3D-tPOP	2.38	1.46	0.94	25.8
3D-tPOP-NaCl-0.25	3.24	1.36	0.62	41.0
3D-tPOP-NaCl-0.5	3.69	1.83	1.02	39.3
3D-tPOP-NaCl-1.0	5.02	3.41	1.06	40.6
3D-tPOP-NaCl-1.5	3.86	2.27	1.12	43.2
3D-tPOP-NaCl-2.0	4.42	2.62	1.29	42.1

[a]The Q_{st} values were calculated from CO_2 uptake isotherms obtained at 273, 298, and 323 K temperatures by applying the Clausius−Clapeyron equation.[43] The Q_{st} values are reported at zero coverage.

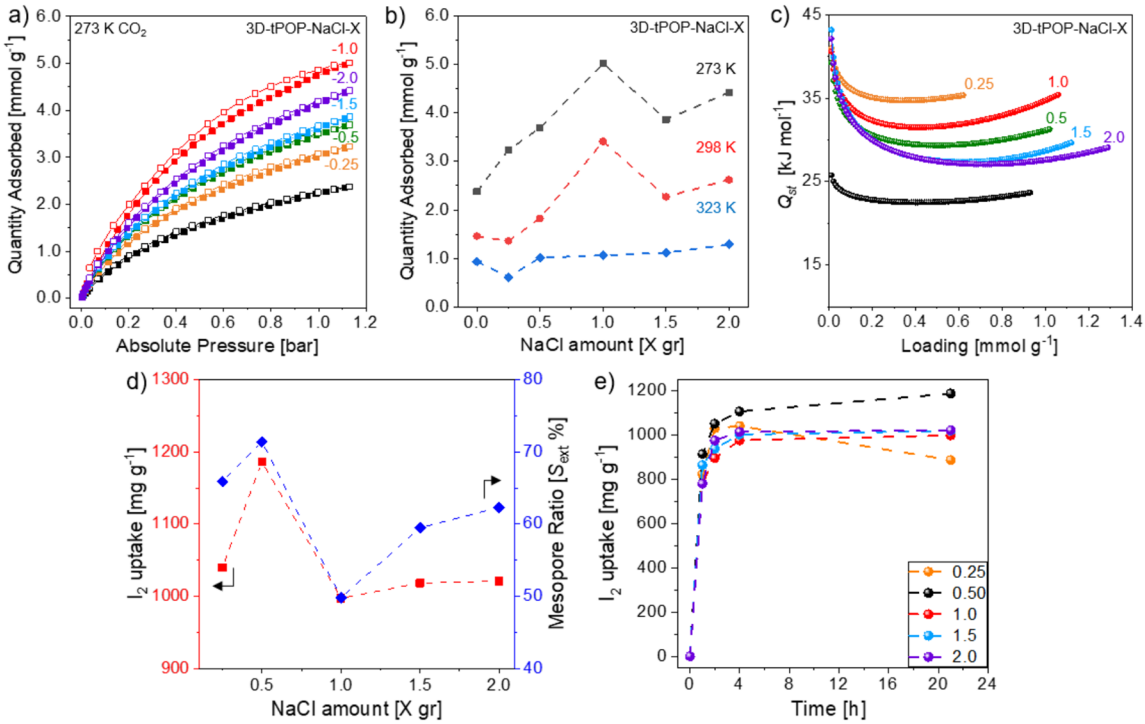

Figure 4. CO_2 and I_2 capture performances of 3D-tPOPs: (a) CO_2 adsorption−desorption isotherms of the 3D-tPOP and 3D-tPOP-NaCl samples obtained at 273 K. Filled and empty symbols correspond to adsorption and desorption, respectively. The values next to the isotherms represent the amount of NaCl template used in grams. (b) Relationship between the CO_2 uptake capacity (mmol g^{-1}) at different temperatures and the NaCl amount. (c) Q_{st} plots of the 3D-tPOP-NaCl samples. (d) I_2 uptake capacity versus NaCl template amount in correlation with the mesopore content [S_{ext} (%); Table 1] of the 3D-tPOPs. (e) I_2 uptake versus time curve of the 3D-tPOPs.

increases the accessibility of ultramicropores but also facilitates efficient mass transport, thus leading to the highest I_2 uptake capacity for 3D-tPOP-NaCl-0.5. 3D-tPOP-NaCl-0.25 was the first to saturate after 4 h because of its lower surface area compared to the other 3D-tPOPs-NaCl, and then it started to lose some of the captured I_2 over time under constant heating. We also tested the reversibility of the I_2 uptake by immersing the polymers into acetone and also by performing TGA measurements after I_2 capture. 3D-tPOPs can be recovered readily both in solution and upon thermal treatment (Figures S23 and S24). We also showed (Figure S25) the reversibility of the I_2 uptake of 3D-tPOPs up to five cycles. As expected, 3D-tPOPs-NaCl showed very similar uptake capacities without any significant loss in the I_2 capture capacity, further proving their reusability. These results showed that the binding of I_2 is physical, and it can be removed easily from the pores because of the lack of charged moieties and relatively polar nature of the functional groups in 3D-tPOPs. The obtained results show another aspect of porosity control, where the presence of mesopores plays a more important role toward I_2 capture. These results also demonstrate that the salt-templated synthesis of POPs is a highly versatile approach for targeting multiple applications by simply changing the template amount. These results demonstrate that, by using a simple and readily available NaCl template, it is possible to design POPs, which can be tailored according to the desired application. In this direction, we have shown that, whereas 1.0 g of template can lead to a higher ratio of micropore, which is essential for CO_2 uptake, 0.5 g of template can produce a higher mesopore ratio for efficient I_2 capture.

3. CONCLUSION

We have demonstrated that hard templates such as NaCl can be used as structural templates for the synthesis of POPs under solvothermal conditions. By systematically controlling the porosity and micropore/mesopore ratio of POPs through template loading, we were able to achieve the desired porosities for highly efficient CO_2 and I_2 capture without altering the chemical structure of the polymers. In a broader context, our strategy offers a universal approach to controlling the porosity and uptake properties of POPs by simply altering the template amount starting from the same monomer and can be applied to various POPs synthesized under solvothermal conditions.

4. EXPERIMENTAL SECTION

Materials and Methods. The synthesis and additional structural characterization data for OTMSTP are provided in the Supporting Information. TFPN was purchased from FluoroChem and used as is. The reaction's solvents and TBAF (1 M in THF) were purchased from Sigma-Aldrich. The NaCl template was purchased from Acros Chemicals. All other solvents were purchased from Fischer Chemicals. All air- and moisture-sensitive chemicals were stored and manipulated in the glovebox. All anhydrous and air/moisture-sensitive solvents were transferred using syringe or cannula via rubber septa. Column chromatography was performed using 230−400 mesh silica (silicyl). Thin-layer chromatography was executed on Merck 60 F_{254} silica gel plates. The ^{1}H and ^{13}C NMR spectra were recorded on Bruker 400 and 500 MHz Avance III spectrometers. The NMR spectra were calibrated based on the deuterated solvent peak. Anhydrous solvents were purchased from Sigma-Aldrich and Acros Chemicals and used as is. Carbon-film-coated copper 250-mesh TEM grids were obtained from Agar Scientific.

Materials Characterization. FTIR spectra were obtained with a PerkinElmer Frontier spectrometer using KBr (Sigma-Aldrich) pellets. The XRD patterns were recorded on a STOE STADI-P system using a Cu Kα_1 incident beam in transmission mode between $2\theta = 2°$ and 40°. XPS analysis was performed on a PHI VersaProbe II scanning XPS microprobe (Physical Instruments AG, Germany). XPS measurements were obtained using a monochromatic Al Kα X-ray source of 24.8 W power with a beam size of 100 μm. The spherical capacitor analyzer was set at a 45° takeoff angle with respect to the sample surface. The pass energy was 46.95 eV, yielding a full width at half-maximum of 0.91 eV for the Ag $3d_{5/2}$ peak (Figure S8). The XPS spectra were fitted using the *fityk* software. TGA measurements were carried on a Mettler-Toledo TGA/DSC 3+ instrument with a heating rate of 3 K min^{-1} using standard 70 μL alumina crucibles with a 20 sccm (air or nitrogen) flow rate. The N_2 and CO_2 sorption measurements were performed on a Micromeritics 3Flex instrument, and the samples were evacuated at 363 K for 12 h prior to the measurements. PSD analysis of the polymers was obtained via the NLDFT model using *SAIEUS* software. The SEM micrographs were recorded using a ThermoFischer Scios 2 focused-ion-beam scanning electron microscope with a 3.0 kV voltage and a 0.40 nA current. The samples were sputtered with 3.0 nm gold on a Cressington 208HR sputtering tool to prevent charging during imaging. The TEM samples were prepared by dispersing polymers in ethanol with subsequent sonication. Then 20 μL of polymer solutions was drop-casted onto the copper TEM grids coated with a carbon film and dried under vacuum. The TEM micrographs were recorded on a FEI Tecnai Osiris instrument using a 120 kV accelerating voltage. CHN EA analysis was carried out using a ThermoFischer Flash 2000 CHNS-O analyzer by utilizing BBOT as a reference standard. The ^{13}C CP-MAS NMR spectra were recorded on a Bruker Avance Neo 400 MHz spectrometer by spinning the samples at a 10 kHz spinning rate.

Synthesis of the POPs. A mixture of 20.2 mg of OTMSTP (0.02 mmol, 1.0 equiv) and 8.0 mg of TFPN (0.04 mmol, 2.0 equiv) was transferred into a Pyrex ampule (18 mL), and 1.0 mL of a mixture of 1:1 dioxane/mesitylene was added. Then, 0.1 mL of TBAF (1 M in THF, 0.1 mmol, 5.0 equiv) and respective amounts of the NaCl template (0.25 to 2.0 gr) were added, and the ampule was freeze-dried in liquid nitrogen. The contents of the ampule was evacuated in a freeze-dried state for 45 min, then sealed by flame, and heated in an oven at 120 °C for 72 h. After the reaction was complete, the solid was filtered out and washed with acetone (100 mL), THF (100 mL), methanol (100 mL), and deionized (DI) water, respectively. Then, the polymers were transferred into a beaker filled with 500 mL of DI water and stirred for 5 days to remove the inorganic salts from the pores. DI water-washed polymers were filtered out and stirred in 500 mL of THF for an additional 3 days. Finally, POPs were isolated by fritted glass filtration and dried under vacuum at 90 °C prior to their characterization.

I_2 Uptake Experiments. Vapor-phase I_2 uptake measurements were performed by simulating the typical nuclear waste processing conditions.[54] In a typical experiment, ~10 mg of the sample was weighed into a ceramic crucible, and then the crucible was loaded into a larger vessel containing I_2 powder. Afterward, the vessel was sealed and heated at 80 °C in a sand bath. At particular time intervals, the crucible was removed, cooled to room temperature, and weighed. The uptake capacity was calculated by subtracting the initial mass and dividing the result by the initial mass: $(m_t - m_0)/m_0$. The samples were recycled by washing with acetone and reused for further I_2 uptake experiments.

■ ASSOCIATED CONTENT

Supporting Information

The Supporting Information is available free of charge at https://pubs.acs.org/doi/10.1021/acsanm.2c00035.

Experimental synthesis procedures, ^1H and ^{13}C NMR spectra for all compounds (Figures S1−S5), additional supporting data for 3D-tPOPs (Figures S6−S25), and EA and a comparison of the CO_2 capture and I_2 uptake performances of 3D-tPOPs with previously reported literature (Tables S1−S3) (PDF)

■ AUTHOR INFORMATION

Corresponding Author

Ali Coskun − *Department of Chemistry, University of Fribourg, Fribourg 1700, Switzerland;* orcid.org/0000-0002-4760-1546; Email: ali.coskun@unifr.ch

Authors

Timur Ashirov − *Department of Chemistry, University of Fribourg, Fribourg 1700, Switzerland*

Kyung Seob Song − *Department of Chemistry, University of Fribourg, Fribourg 1700, Switzerland*

Complete contact information is available at: https://pubs.acs.org/10.1021/acsanm.2c00035

Author Contributions

T.A. performed all of the experiments. K.S.S. helped to analyze the sorption properties of the samples. A.C. conceived and supervised the project, procured funds, and wrote the manuscript together with T.A and K.S.S.

Notes

The authors declare no competing financial interest.

■ ACKNOWLEDGMENTS

The authors acknowledge support from the Swiss National Science Foundation for funding of this research (Grant 200021-175947).

■ REFERENCES

(1) Opoku, E. E. O.; Boachie, M. K. The environmental impact of industrialization and foreign direct investment. *Energy Policy* **2020**, *137*, 111178.

(2) Hidalgo, D.; Martín-Marroquín, J. M. Power-to-methane, coupling CO_2 capture with fuel production: An overview. *Renew. Sust. Energy Rev.* **2020**, *132*, 110057.

(3) Espinal, L.; Poster, D. L.; Wong-Ng, W.; Allen, A. J.; Green, M. L. Measurement, Standards, and Data Needs for CO_2 Capture Materials: A Critical Review. *Environ. Sci. Technol.* **2013**, *47* (21), 11960−11975.

(4) Singh, G.; Lee, J.; Karakoti, A.; Bahadur, R.; Yi, J.; Zhao, D.; AlBahily, K.; Vinu, A. Emerging trends in porous materials for CO_2 capture and conversion. *Chem. Soc. Rev.* **2020**, *49* (13), 4360−4404.

(5) Zou, L.; Sun, Y.; Che, S.; Yang, X.; Wang, X.; Bosch, M.; Wang, Q.; Li, H.; Smith, M.; Yuan, S.; Perry, Z.; Zhou, H.-C. Porous Organic Polymers for Post-Combustion Carbon Capture. *Adv. Mater.* **2017**, *29* (37), 1700229.

(6) Bhanja, P.; Modak, A.; Bhaumik, A. Porous Organic Polymers for CO_2 Storage and Conversion Reactions. *ChemCatChem.* **2019**, *11* (1), 244−257.

(7) Patel, H. A.; Byun, J.; Yavuz, C. T. Carbon Dioxide Capture Adsorbents: Chemistry and Methods. *ChemSusChem* **2017**, *10* (7), 1303−1317.

(8) Byun, Y.; Je, S. H.; Talapaneni, S. N.; Coskun, A. Advances in Porous Organic Polymers for Efficient Water Capture. *Chem. Eur. J.* **2019**, *25* (44), 10262−10283.

(9) Fritz, P. W.; Coskun, A. The Prospect of Dimensionality in Porous Semiconductors. *Chem. Eur. J.* **2021**, *27* (27), 7489−7501.

(10) Wang, T.-X.; Liang, H.-P.; Anito, D. A.; Ding, X.; Han, B.-H. Emerging applications of porous organic polymers in visible-light photocatalysis. *J. Mater. Chem. A* **2020**, *8* (15), 7003−7034.

(11) Hong, Y.; Rozyyev, V.; Yavuz, C. T. Alkyl-Linked Porphyrin Porous Polymers for Gas Capture and Precious Metal Adsorption. *Small Sci.* **2021**, *1* (6), 2000078.
(12) Kim, J.; Elabd, A.; Chung, S.-Y.; Coskun, A.; Choi, J. W. Covalent Triazine Frameworks Incorporating Charged Polypyrrole Channels for High-Performance Lithium-Sulfur Batteries. *Chem. Mater.* **2020**, *32* (10), 4185−4193.
(13) Das, S.; Heasman, P.; Ben, T.; Qiu, S. Porous Organic Materials: Strategic Design and Structure-Function Correlation. *Chem. Rev.* **2017**, *117* (3), 1515−1563.
(14) Talapaneni, S. N.; Lee, J. H.; Je, S. H.; Buyukcakir, O.; Kwon, T.-w.; Polychronopoulou, K.; Choi, J. W.; Coskun, A. Chemical Blowing Approach for Ultramicroporous Carbon Nitride Frameworks and Their Applications in Gas and Energy Storage. *Adv. Funct. Mater.* **2017**, *27* (1), 1604658.
(15) Kaiser, S. K.; Song, K. S.; Mitchell, S.; Coskun, A.; Pérez-Ramírez, J. Nitrogen-Doped Carbons with Hierarchical Porosity via Chemical Blowing Towards Long-Lived Metal-Free Catalysts for Acetylene Hydrochlorination. *ChemCatChem.* **2020**, *12* (7), 1922−1925.
(16) Wu, D.; Xu, F.; Sun, B.; Fu, R.; He, H.; Matyjaszewski, K. Design and Preparation of Porous Polymers. *Chem. Rev.* **2012**, *112* (7), 3959−4015.
(17) Hentze, H. P.; Antonietti, M. Template synthesis of porous organic polymers. *Curr. Opin. Solid State Mater. Sci.* **2001**, *5* (4), 343−353.
(18) Maschita, J.; Banerjee, T.; Savasci, G.; Haase, F.; Ochsenfeld, C.; Lotsch, B. V. Ionothermal Synthesis of Imide-Linked Covalent Organic Frameworks. *Angew. Chem., Int. Ed.* **2020**, *59* (36), 15750−15758.
(19) Song, K. S.; Talapaneni, S. N.; Ashirov, T.; Coskun, A. Molten Salt Templated Synthesis of Covalent Isocyanurate Frameworks with Tunable Morphology and High CO2 Uptake Capacity. *ACS Appl. Mater. Interfaces* **2021**, *13* (22), 26102−26108.
(20) Troschke, E.; Grätz, S.; Borchardt, L.; Haubold, D.; Senkovska, I.; Eychmueller, A.; Kaskel, S. Salt templated synthesis of hierarchical covalent triazine frameworks. *Microporous Mesoporous Mater.* **2017**, *239*, 190−194.
(21) Chen, J.; Qiu, T.; Yan, W.; Faul, C. F. J. Exploiting Hansen solubility parameters to tune porosity and function in conjugated microporous polymers. *J. Mater. Chem. A* **2020**, *8* (43), 22657−22665.
(22) Chen, J.; Yan, W.; Townsend, E. J.; Feng, J.; Pan, L.; Del Angel Hernandez, V.; Faul, C. F. J. Tunable Surface Area, Porosity, and Function in Conjugated Microporous Polymers. *Angew. Chem., Int. Ed.* **2019**, *58* (34), 11715−11719.
(23) Li, J.; Ren, H.; Zou, X.; Cai, K.; Zhao, N.; Zhu, G. Hard-template synthesis of micro-mesoporous organic frameworks with controlled hierarchicity. *Chem. Commun.* **2018**, *54* (60), 8335−8338.
(24) Shi, X.; Ma, D.; Xu, F.; Zhang, Z.; Wang, Y. Table-salt enabled interface-confined synthesis of covalent organic framework (COF) nanosheets. *Chem. Sci.* **2020**, *11* (4), 989−996.
(25) Talapaneni, S. N.; Kim, J.; Je, S. H.; Buyukcakir, O.; Oh, J.; Coskun, A. Bottom-up synthesis of fully sp^2 hybridized three-dimensional microporous graphitic frameworks as metal-free catalysts. *J. Mater. Chem. A* **2017**, *5* (24), 12080−12085.
(26) Byun, Y.; Xie, L. S.; Fritz, P.; Ashirov, T.; Dincă, M.; Coskun, A. A Three-Dimensional Porous Organic Semiconductor Based on Fully sp^2-Hybridized Graphitic Polymer. *Angew. Chem., Int. Ed.* **2020**, *59* (35), 15166−15170.
(27) Dogan, N. A.; Hong, Y.; Ozdemir, E.; Yavuz, C. T. Nanoporous Polymer Microspheres with Nitrile and Amidoxime Functionalities for Gas Capture and Precious Metal Recovery from E-Waste. *ACS Sustain. Chem. Eng.* **2019**, *7* (1), 123−128.
(28) Kabir, S. M. H.; Iyoda, M. Selective Synthesis of Tetraphenylenes and Biphenylenes Using Copper-Catalyzed Coupling of Zincacyclopentadienes. *Synthesis* **2000**, *2000* (13), 1839−1842.
(29) Li, X.; Han, J.-W.; Wong, H. N. C. Palladium-Catalyzed Double Ullmann Reaction: An Approach towards Tetraphenylenes. *Asian J. Org. Chem.* **2016**, *5* (1), 74−81.
(30) Zhang, B.; Wei, M.; Mao, H.; Pei, X.; Alshmimri, S. A.; Reimer, J. A.; Yaghi, O. M. Crystalline Dioxin-Linked Covalent Organic Frameworks from Irreversible Reactions. *J. Am. Chem. Soc.* **2018**, *140* (40), 12715−12719.
(31) Guodong, W.; Yongcai, S.; Yongqiang, L. Evolution of molecular composition of polycarbosilane and its effect on spinnability. *RSC Adv.* **2018**, *8* (39), 21863−21870.
(32) Byun, Y.; Coskun, A. Epoxy-Functionalized Porous Organic Polymers via the Diels-Alder Cycloaddition Reaction for Atmospheric Water Capture. *Angew. Chem., Int. Ed.* **2018**, *57* (12), 3173−3177.
(33) Smith, A. L. *Analysis of silicones*; Wiley: New York, 1974.
(34) Moulder, J. F.; Chastain, J. *Handbook of X-ray Photoelectron Spectroscopy: A Reference Book of Standard Spectra for Identification and Interpretation of XPS Data*; Physical Electronics Division, Perkin-Elmer Corp., 1992.
(35) López, G. P.; Castner, D. G.; Ratner, B. D. XPS O 1s binding energies for polymers containing hydroxyl, ether, ketone and ester groups. *Surf. Interface Anal.* **1991**, *17* (5), 267−272.
(36) Brunauer, S.; Emmett, P. H.; Teller, E. Adsorption of Gases in Multimolecular Layers. *J. Am. Chem. Soc.* **1938**, *60* (2), 309−319.
(37) Lowell, S.; Shields, J. E.; Thomas, M. A.; Thommes, M. *Characterization of Porous Solids and Powders: Surface Area, Pore Size and Density*; Springer, 2006.
(38) Sing, K. S. W. Reporting physisorption data for gas/solid systems with special reference to the determination of surface area and porosity (Recommendations 1984). *Pure Appl. Chem.* **1985**, *57* (4), 603−619.
(39) Mecozzi, S.; West, A. P.; Dougherty, D. A. Cation-π Interactions in Simple Aromatics: Electrostatics Provide a Predictive Tool. *J. Am. Chem. Soc.* **1996**, *118* (9), 2307−2308.
(40) Barrett, E. P.; Joyner, L. G.; Halenda, P. P. The Determination of Pore Volume and Area Distributions in Porous Substances. I. Computations from Nitrogen Isotherms. *J. Am. Chem. Soc.* **1951**, *73* (1), 373−380.
(41) Eysseltová, J.; Málková, Z. Solubility in the Systems MCl (M = Na, K)-1,4-Dioxane-Water at 25 °C. *J. Solution Chem.* **2006**, *35* (9), 1329−1334.
(42) Chang, N. N.; Daly, S. R.; Girolami, G. S. Salt elimination reactions do not always eliminate. Mechanistic study of the reaction of $NdCl_3$ with sodium N,N-dimethylaminodiboranate. *Polyhedron* **2019**, *162*, 52−58.
(43) Dawson, R.; Adams, D. J.; Cooper, A. I. Chemical tuning of CO_2 sorption in robust nanoporous organic polymers. *Chem. Sci.* **2011**, *2* (6), 1173−1177.
(44) Durá, G.; Budarin, V. L.; Castro-Osma, J. A.; Shuttleworth, P. S.; Quek, S. C. Z.; Clark, J. H.; North, M. Importance of Micropore-Mesopore Interfaces in Carbon Dioxide Capture by Carbon-Based Materials. *Angew. Chem., Int. Ed.* **2016**, *55* (32), 9173−9177.
(45) Zhang, H.; Wang, Z.; Luo, X.; Lu, J.; Peng, S.; Wang, Y.; Han, L. Constructing Hierarchical Porous Carbons With Interconnected Micro-mesopores for Enhanced CO_2 Adsorption. *Front. Chem.* **2020**, *7*, 919.
(46) Zhang, Z.; Zhou, J.; Xing, W.; Xue, Q.; Yan, Z.; Zhuo, S.; Qiao, S. Z. Critical role of small micropores in high CO_2 uptake. *Phys. Chem. Chem. Phys.* **2013**, *15* (7), 2523−2529.
(47) Lü, J.; Perez-Krap, C.; Suyetin, M.; Alsmail, N. H.; Yan, Y.; Yang, S.; Lewis, W.; Bichoutskaia, E.; Tang, C. C.; Blake, A. J.; Cao, R.; Schröder, M. A Robust Binary Supramolecular Organic Framework (SOF) with High CO_2 Adsorption and Selectivity. *J. Am. Chem. Soc.* **2014**, *136* (37), 12828−12831.
(48) Dong, A.; Zhu, Y.; Ren, M.; Sun, X.; Murugadoss, V.; Yuan, Y.; Wen, J.; Wang, X.; Chen, Q.; Guo, Z.; Wang, N. Remarkably Enhanced CO_2 Uptake and Uranium Extraction by Functionalization of Cyano-bearing Conjugated Porous Polycarbazoles. *Eng. Sci.* **2019**, *6*, 44−52.

(49) Ashirov, T.; Alrayyani, M.; Song, K.-S.; Miljanić, O. Š.; Coskun, A. Cyclotetrabenzil-Based Porous Organic Polymers with High Carbon Dioxide Affinity. *Org. Mater.* **2021**, *03* (02), 346–352.
(50) Riley, B. J.; Vienna, J. D.; Strachan, D. M.; McCloy, J. S.; Jerden, J. L. Materials and processes for the effective capture and immobilization of radioiodine: A review. *J. Nucl. Mater.* **2016**, *470*, 307–326.
(51) Shetty, D.; Raya, J.; Han, D. S.; Asfari, Z.; Olsen, J.-C.; Trabolsi, A. Lithiated Polycalix[4]arenes for Efficient Adsorption of Iodine from Solution and Vapor Phases. *Chem. Mater.* **2017**, *29* (21), 8968–8972.
(52) Skorjanc, T.; Shetty, D.; Sharma, S. K.; Raya, J.; Traboulsi, H.; Han, D. S.; Lalla, J.; Newlon, R.; Jagannathan, R.; Kirmizialtin, S.; Olsen, J.-C.; Trabolsi, A. Redox-Responsive Covalent Organic Nanosheets from Viologens and Calix[4]arene for Iodine and Toxic Dye Capture. *Chem. Eur. J.* **2018**, *24* (34), 8648–8655.
(53) Xie, W.; Cui, D.; Zhang, S.-R.; Xu, Y.-H.; Jiang, D.-L. Iodine capture in porous organic polymers and metal-organic frameworks materials. *Mater. Horiz.* **2019**, *6* (8), 1571–1595.
(54) Walker, S.; Hyde, R. A.; Piper, R. B.; Roy, M. W. An overview of in situ waste treatment technologies. *Spectrum 92: nuclear and hazardous waste management international topical meeting*, Boise, ID, Aug 23–27, 1992; American Nuclear Society, 1992; p 12.
(55) Yan, Z.; Yuan, Y.; Tian, Y.; Zhang, D.; Zhu, G. Highly Efficient Enrichment of Volatile Iodine by Charged Porous Aromatic Frameworks with Three Sorption Sites. *Angew. Chem., Int. Ed.* **2015**, *54* (43), 12733–12737.